Pressure-driven, resistive magnetohydrodynamic interchange instabilities in laser-produced high-energy-density plasmas

C. K. Li,[1,*] J. A. Frenje,[1] R. D. Petrasso,[1] F. H. Séguin,[1] P. A. Amendt,[2] O. L. Landen,[2] R. P. J. Town,[2] R. Betti,[3,†] J. P. Knauer,[3] D. D. Meyerhofer,[3,†] and J. M. Soures[3]

[1]*Plasma Science and Fusion Center, Massachusetts Institute of Technology, Cambridge, Massachusetts 02139, USA*

[2]*Lawrence Livermore National Laboratory, Livermore, California 94550, USA*

[3]*Laboratory for Laser Energetics, University of Rochester, Rochester, New York 14623, USA*

(Received 30 March 2009; published 15 July 2009)

Recent experiments using proton backlighting of laser-foil interactions provide unique opportunities for studying magnetized plasma instabilities in laser-produced high-energy-density plasmas. Time-gated proton radiograph images indicate that the outer structure of a magnetic field entrained in a hemispherical plasma bubble becomes distinctly asymmetric after the laser turns off. It is shown that this asymmetry is a consequence of pressure-driven, resistive magnetohydrodynamic (MHD) interchange instabilities. In contrast to the predictions made by ideal MHD theory, the increasing plasma resistivity after laser turn-off allows for greater low-mode destabilization ($m>1$) from reduced stabilization by field-line bending. For laser-generated plasmas presented herein, a mode-number cutoff for stabilization of perturbations with $m>\sim[8\pi\beta(1+D_m k_\perp^2 \gamma_{\max}^{-1})]^{1/2}$ is found in the linear growth regime. The growth is measured and is found to be in reasonable agreement with model predictions.

DOI: 10.1103/PhysRevE.80.016407 PACS number(s): 52.38.Fz, 52.50.Jm, 52.70.Nc

I. INTRODUCTION

Pressure-driven, resistive interchange modes are fundamental magnetohydrodynamic (MHD) instabilities in plasmas [1–4]. These convective instabilities occur under circumstances with unfavorable field curvature relative to the pressure gradient ($\boldsymbol{\kappa}\cdot\nabla P>0$, where $\boldsymbol{\kappa}=\boldsymbol{B}\cdot\nabla\boldsymbol{B}/B^2$ is the line curvature of the magnetic (B) field and ∇P is the plasma pressure gradient). In this configuration, field lines are concave toward the plasma and have tension, which tends to make them shorten and collapse inward, while plasma pressure has a natural tendency to expand outward. Unstable perturbations, which have short wavelengths perpendicular to the B field ($k_\perp L_p \gg 1$, where $L_p \equiv P/\nabla P$ is the pressure scale length) and long wavelengths parallel to the field ($k_\parallel$), grow and result in interchanges of field and their plasma content between the inside and outside of the plasma edge, leading to a state of lower internal energy. The instabilities evolve through a linear growth phase followed by a nonlinear one [3,4]. The basic behavior of these unstable modes is analogous to the Rayleigh-Taylor instabilities, which are driven by acceleration (equivalent to the pressure gradient here for interchange instabilities) in plasmas [3,4]. Interchange instabilities have been widely studied in the magnetically confined tenuous plasmas [1–4], but have not been explored, to our knowledge, in high-temperature, dense high-energy-density (HED) plasmas [5].

Laser-produced plasmas are typical HED plasmas with thermal and/or magnetic pressures >1 Mbar [5]. Generated by a circular laser beam interacting with a solid foil, a plasma bubble [6–9] is similar to those plasmas confined by a typical Z pinch. Ideal MHD theory [3], which ignores plasma resistivity, predicts that the only unstable interchange modes are the $m=0$ (sausage instability) and the $m=1$ (kink instability), while the other $m>1$ modes are stabilized because their growth is energetically unfavorable in overcoming the tension generated by the curvature of B-field lines ($\propto B^2/r$). The stabilizing field-line bending effect can be significantly reduced in resistive plasmas, since the plasma resistivity results in field slipping and diffusion across the plasma boundary, allowing high-mode-number modes to be destabilized and grow. This scenario is illustrated schematically in Fig. 1.

We recently reported an observation of such an edge asymmetry in laser-produced plasmas from proton radiography of laser-foil interactions [6]. Largely based on conceptual arguments and order-of-magnitude estimates, therein it was conjectured that this asymmetric structure was a consequence of pressure-driven, resistive MHD interchange instabilities. This hypothesis is made quantitative and more rigorous in this paper. The generation of laser-produced spontaneous magnetic fields is outlined in Sec. II. Section III

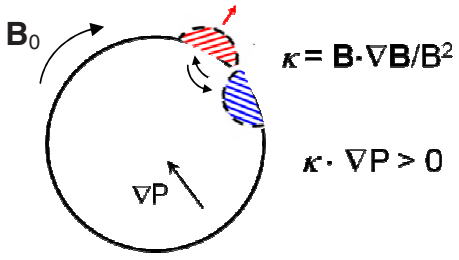

FIG. 1. (Color online) Top view (cartoon) of a laser generated plasma bubble illustrating schematically a high-mode-number ($m>1$), pressure-driven, resistive MHD interchange instability resulting in an interchange of fields between the inside (blue color) and outside (red color) of the bubble edge. The diffusion of the B field reduces the effect of field-line bending. The B_0 represents the undisturbed B field.

*li@psfc.mit.edu

†Also at Department of Mechanical Engineering, Physics and Astronomy, University of Rochester, Rochester, New York.

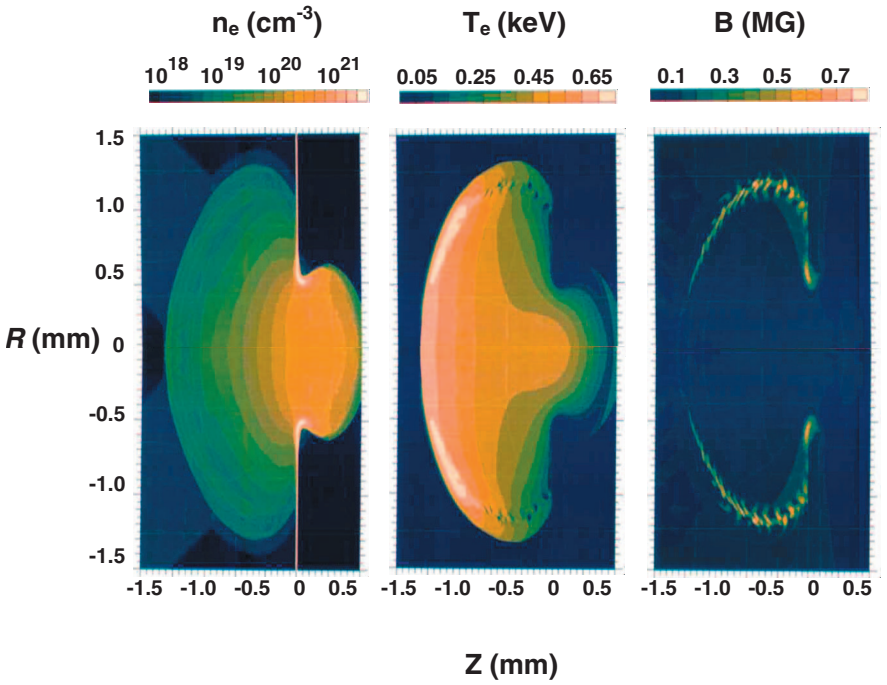

FIG. 2. (Color) Side view of the distributions of n_e, T_e, and B-field amplitude in an isolated laser-generated plasma bubble at $t=1.8$ ns for a 1 ns laser drive pulse with beam spot size ~ 800 μm in diameter, simulated with the 2D code LASNEX. The surface of the foil is at position Z=0.0 on the horizontal axes and the laser is incident from the left. The field is always perpendicular to the plane of the image.

presents theoretical description of the features of interchange modes in HED plasmas. The experimental results and discussions are presented in Sec. IV. The important findings are summarized in Sec. V.

II. LASER-PRODUCED HIGH-ENERGY-DENSITY PLASMAS AND SPONTANEOUS MAGNETIC FIELDS

Laser-generated plasmas are transient with durations of order nanoseconds. High plasma densities ($>\sim 10^{18}$ cm^{-3}) and high temperatures (~ 1 keV), intense self-generated B fields (~ 1 MG), and high ratios of thermal pressure to magnetic pressure ($\beta \gg 1$) distinguish this from the tenuous plasmas of order 10^{14} cm^{-3} or lower, which are characteristics of most magnetic-confinement experiments. For long-pulse, low-intensity laser light, the dominant source for B field generation is noncollinear electron density and temperature gradients ($\nabla n_e \times \nabla T_e$) [10–12]. In the regime with low ionization state Z and high temperature where resistivity is low, B-field growth is linear in time and is balanced by convective transport [10–12] $\nabla \times (\boldsymbol{v} \times \boldsymbol{B})$, where $\boldsymbol{v}$ is the plasma fluid velocity; i.e., the B field is "frozen in." When the laser is off and the cooling plasma becomes more resistive, field diffusion dominates convective transport [10–12] [$\nabla \times (D_m \nabla \times \boldsymbol{B})$, where D_m is the magnetic diffusion coefficient]. Under these circumstances, B-field generation and evolution are governed by [10–12]

$$\frac{\partial \boldsymbol{B}}{\partial t} \approx \nabla \times (\boldsymbol{v} \times \boldsymbol{B}) - \frac{1}{en_e} \nabla n_e \times \nabla T_e - \nabla \times (D_m \nabla \times \boldsymbol{B}). \tag{1}$$

Figure 2 shows the spatial distributions of electron density (n_e), temperature (T_e), and B field in a plasma bubble due to the interaction of a laser beam (wavelength=0.351 nm, 1 ns pulse with beam spot size ~ 800 μm in diameter and energy ~ 400 J), with a 5-μm-thick plastic (CH) foil at a time of 1.8 ns, simulated by the two-dimensional (2D) radiation-hydrodynamics code LASNEX [13,14]. The maximum field strength occurs around the surface of the hemispherical plasma bubble due to the largest temperature gradients occurring around the bubble's edge. The relative importance of plasma convection to diffusion during field evolution is characterized by the magnetic Reynolds number,

$$R_m = \frac{L_\perp v}{D_m} \approx \left| \frac{\nabla \times (\boldsymbol{v} \times \boldsymbol{B})}{\nabla \times (D_m \nabla \times \boldsymbol{B})} \right|, \tag{2}$$

where $L_\perp$ is a characteristic length scale [3,4]. When the laser is on, $R_m \gg 1$, so the fields must be frozen in and move with the plasmas (For example, taking a characteristic scale length $L_\perp \approx T_e / \nabla T_e \sim 100$ μm, a bubble expansion velocity $v \sim 5 \times 10^7$ cm s^{-1}, and a diffusion $D_m \sim 4 \times 10^2$ cm^2 s^{-1}, one has $R_m \sim 1000$.) The flow is dominated by plasma fluid dynamics and is insignificantly affected by the fields despite their MG levels [6–8,15]. The bubble expansion in this regime can be approximated as "free streaming" because the velocity is of the order of the ion sound velocity ($C_s \sim 2 \times 10^7$ cm s^{-1}). After the laser pulse turns off (the energy input is stopped) the plasma bubble continues to expand and begins to cool. The cooling plasma becomes more collisional and increasingly resistive. This allows the field to diffuse across the plasma boundary and eventually dissipate. At these postdriven times, the fluid behavior near the plasma edge is increasingly governed by the field and resistive effects (i.e., $R_m < 1$) and the local plasma β becomes of order 1 [6–8,15]. As will be shown, this gives rise to pressure-driven resistive instabilities. The large amplitudes of unstable modes, resulting from exponential growth around the plasma bubble edge, provide unique opportunities for the experimental study of such important instabilities in HED plasmas.

III. PRESSURE-DRIVEN RESISTIVE INSTABILITIES

In analyzing the instabilities in the linear growth phase, it is assumed that the perturbations are small so that the linearized MHD equations can be used to elucidate the fundamental features of the instabilities. Considering the small-scale modes ($k_\perp L_p \gg 1$), linearizing the equations ($\partial/\partial t \to \gamma$, where γ is the growth rate) and Fourier transforming the perturbations ($\nabla \to i\boldsymbol{k}$), a set of algebraic high-β reduced MHD eigenequations is obtained [4]. By solving for the eigenvalues, a dispersion relation for the mode growth rate is obtained [4],

$$\gamma^2 \approx \frac{2(\boldsymbol{B}\cdot\nabla\boldsymbol{B})\,\nabla P}{\rho B^2} - \frac{k_\parallel^2 v_A^2}{1 + D_m k_\perp^2 \gamma^{-1}}. \tag{3}$$

In this dispersion equation, the second term represents the mode stabilization due to field-line bending. Perturbations are stabilized when

$$\frac{2(\boldsymbol{B}\cdot\nabla\boldsymbol{B})\,\nabla P}{\rho B^2} \le \frac{k_\parallel^2 v_A^2}{1 + D_m k_\perp^2 \gamma^{-1}}, \tag{4}$$

where

$$v_A = \sqrt{\frac{B^2}{\rho}} \tag{5}$$

is the Alfven speed and the wave number along the toroidal B field is

$$k_\parallel = \frac{m}{2\pi R}, \tag{6}$$

where m is the mode number. As illustrated in Fig. 2, the scale length of the temperature is about 30% of the bubble radius, i.e., $L_T \sim 0.3 \times R$. The wave number perpendicular to the field line is given as approximately $k_\perp \sim L_B^{-1}$ ($L_B \equiv B/\nabla B \sim 0.1 \times R$). Considering $\nabla \sim L_T^{-1}$, the field-line curvature is approximately

$$|\boldsymbol{\kappa}| = \left|\frac{\boldsymbol{B}\cdot\nabla\boldsymbol{B}}{B^2}\right| \sim \frac{1}{L_T}. \tag{7}$$

The magnetic diffusion coefficient is

$$D_m = \frac{c^2}{4\pi}\eta, \tag{8}$$

where η is the plasma resistivity. Using $L_T \sim 0.3R$, the dispersion relation [Eq. (3)] can be rewritten as

$$\gamma^2 \sim \frac{2P}{\rho L_T^2} - \frac{m^2 B^2}{\rho(2\pi R)^2(1 + D_m k_\perp^2 \gamma^{-1})} \sim \frac{2B^2\beta}{\rho\pi R^2} - \frac{m^2 B^2}{4\rho\pi^2 R^2(1 + D_m k_\perp^2 \gamma^{-1})}. \tag{9}$$

When $\gamma^2 \le 0$, the (minimum) condition for perturbation stabilization due to the effects of field-line bending becomes

$$\beta - \frac{m^2}{8\pi(1 + D_m k_\perp^2 \gamma_{\max}^{-1})} \le 0, \tag{10}$$

or

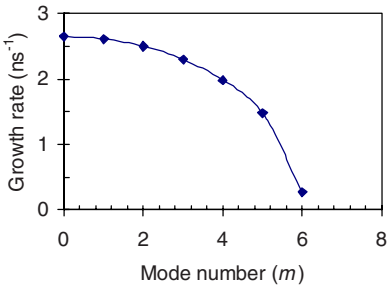

FIG. 3. (Color online) Growth rate determined using Eq. (3) is plotted as a function of the mode number for the plasma conditions discussed in this paper showing that the effects of stabilization will be cut off at $m \sim 6$.

$$m > \sim \sqrt{8\pi\beta(1 + D_m k_\perp^2 \gamma_{\max}^{-1})}, \tag{11}$$

where

$$\gamma_{\max} = \gamma|_{m=0} \tag{12}$$

is the maximum growth rate that occurs when $m=0$, i.e., sausage instability. As indicated by Eq. (3), the effect of field-line bending on stabilizing perturbations will be significantly reduced when $D_m k_\perp^2 \gamma^{-1} \ge 1$ [4].

When compared to typical tenuous plasmas with low plasma β's ($\sim \ll 1$), typical laser-produced HED plasmas have, as discussed in the previous section, relatively large plasma β's, allowing a much higher mode number cutoff for stabilizing perturbations. For physical quantities of experiments relevance to the laser-foil interactions [6–8,15] on the OMEGA laser facility [16] (taking typical values in the region around the plasma edge after the laser turns off (Fig. 2), $n_i \sim 1 \times 10^{18}$ cm^{-3}, $n_e \approx Zn_i \sim 3.5 \times 10^{18}$ cm^{-3}, $T_e \sim 0.4$ keV, and $B \sim 0.3$ MG) $\beta \sim 1$, with an estimated mode number cutoff of $m \sim 6$. Inserting these numbers in Eq. (9), the growth rate as a function of the mode numbers is plotted in Fig. 3.

After evolving through a linear regime, the growth of instabilities enters a nonlinear phase. In this phase, the unstable perturbations in the outward motion move into a region with reduced ambient pressure resulting in the reduction in plasma density around the apex [4] and the reduction in B field (causing a reduction in the field-line bending). These self-focusing effects tend to drive instabilities nonlinearly leading to explosive growth [17]. Conversely, the nonlinear effects of inward motion of unstable perturbations tend to be stabilized resulting from the field compression and plasma flow into the valleys [17]. The combined effects result in a fingerlike structure: an explosive growth of outward instabilities and stabilized inward perturbations [4].

IV. EXPERIMENTS AND DISCUSSIONS

A. Experiments

These pressure-driven, resistive instabilities were studied with monoenergetic proton radiography [6–9,15,18], as shown schematically in Fig. 4, using a backlighter that produced pulsed protons at the discrete energy of 15 MeV

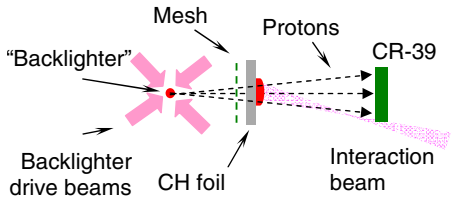

FIG. 4. (Color online) Schematic of the experiment setup for face-on proton radiography. Distances from the backlighter are 1.3 cm for the mesh, 1.5 cm for the CH foil (5 μm thick), and 30 cm for the CR-39 detector [6].

(fusion products of the nuclear reaction $D+{}^3He \rightarrow \alpha+p$, generated from D ^{3}He-filled, thin-glass-shell implosions driven by 20 OMEGA laser beams [16]). Plasmas and B fields were generated through laser-plasma interactions on a plastic (CH) foil by a single laser beam (henceforth called the *interaction beam*) with a wavelength of 0.351 μm, linearly polarized, and incident at 23° from the normal direction. The 1-ns-long square laser pulse had an energy of ~400 J and a spot diameter of ~800 μm determined by phase plate SG4 (defined as 95% energy deposition) [16,19,20] resulting in a peak laser intensity of order 10^{14} W/cm. The nickel mesh used was 60 μm thick with 150 μm period and 75 μm holes [6–9,15,18] and radiographs were recorded using CR-39 detectors [21]. The duration of each "exposure," determined by the emission time of the backlighter produced protons, was ~130 ps. Since the backlighter-to-foil flight time for the protons was ~0.28 ns, an image representing the state of the field (at the foil at time t_a after the onset of the interaction beam) was made by starting this beam at time t_a+0.28 ns after the mean backlighter production time.

B. Data and discussion

Face-on proton radiograph images are shown in Fig. 5 (Ref. [6]). Each image is labeled with a time that represents the interval between the start of the interaction beam and the arrival of the backlighter protons and shows how the proton beamlets were deflected while passing through the B field that forms around the bubble [22]. The images show that while the laser beam is on ($t<1.2$ ns) the field structure expands approximately in tandem with a hemispherical plasma bubble maintaining 2D cylindrical symmetry. Each image has a sharp circular ring where beamlets pile up after passing through the edges of the bubble where the B fields were largest. This circle is a magnified image of the bubble edge because the angular deflection of each beamlet is proportional to $\int \boldsymbol{B}\times d\ell$ (where $d\ell$ is the differential path length along the proton trajectory) and $\boldsymbol{B}\times d\ell$ points away from the bubble center.

When the laser turns off ($t>1.2$ ns), the bubble continues to expand as the field decays and becomes distinct asymmetric, indicating instability growth. This is contrary to the 2D LASNEX simulations that cannot model three-dimensional (3D) asymmetries. It might be argued that the observation of a 3D structure renders comparison with the 2D simulations irrelevant, but 3D codes are not yet available and it is important to consider only the data at hand. (Work is currently underway on combining the 3D hydro code HYDRA with a field generating package [23]). Experimental measurements such as those shown here are important because they directly reveal previously unpredicted physical phenomena, indicate the fundamental importance of 3D processes in certain regimes (such as in the decay phase), and provide invaluable information for benchmarking a true 3D code. A rough estimate suggests that high-mode-number modes ($m\sim3-6$) occur and are superimposed on the expanding plasma bubble. The time evolution of the imaging spatial structures clearly indicates that these modes are unstable and that their amplitudes grow continuously (Fig. 5). As described in the previous sections, the experimental conditions and plasma bubble configuration satisfy the requirements for the appearance of pressure-driven resistive interchange instabilities: first, the bubble has unfavorable field curvature relative to the pressure gradient ($\kappa\cdot\nabla P>0$) in which field lines are concave toward the plasma and plasma pressure tends to expand outward; second, at these postdriven times, the fluid behavior near the bubble edge is dominated by field and resistive effects. Plasma resistivity significantly reduces the stabilization associated with field-line bending, allowing high-mode-number perturbations ($m>1$) to destabilize and grow. As a consequence, these conditions result in the interchange of fields between the inside and outside of the bubble. Pure fluid instabilities such as the Widnall type [24] might be visible while the laser is on (when B fields do not have much impact on the plasma flow but are frozen in); there is no evidence that this is occurring.

Quantitative comparison of measured time evolution of rms deviations defined as deviation of the outer bubble boundary from the average radii

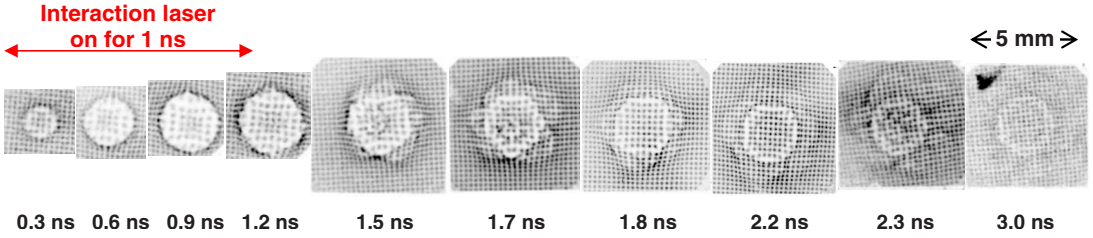

FIG. 5. (Color online) Measured face-on D ^{3}He proton images showing the spatial structure and temporal evolution of B fields generated by laser-plasma interactions. Each image is labeled by the time between the arrival at the foil of the interaction beam and the arrival of the imaging protons. The images illustrate the transition from the 1 ns illumination period (with 2D symmetric expansion of B fields) to a postlaser decay phase with 3D structures emerging around the bubble edge and in the interior as the expanding bubble cools and becomes increasingly resistive.

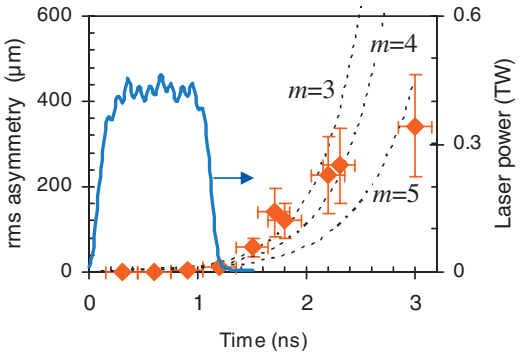

FIG. 6. (Color) Measured time evolution of rms deviations of the outer bubble boundary from the average radii (averaged azimuthally over angles from individual images) are shown to be reasonably consistent with the predicted growth of interchange instabilities. The blue curve is the time history of the laser intensity.

$$\Delta r^2 = \frac{1}{N}\sum_{i}^{N} (r_i - \bar{r})^2, \tag{13}$$

where N is the total number of the deviations, with calculated growth in the linear growth regime [Eq. (3)], is given in Fig. 6. Experimental data are reasonably well reproduced using theoretical predictions and provide compelling evidence in support that they are due to interchange instabilities. This agreement also suggests that the instability has dominant mode numbers $m \sim 3-5$. The measurement uncertainties are large reflecting the uncertainties involved in determining the amplitudes of various perturbation modes. Fingerlike structures associated with nonlinear growth do not appear. This suggests that the fields have dissipated sufficiently before the onset of nonlinear growth. This will be a topic for future study.

V. SUMMARY

Pressure-driven, resistive magnetohydrodynamic interchange instabilities in laser-produced high-energy-density plasmas have been studied with proton radiography. Unstable, high-mode-number perturbations ($m > 1$) occur around the expanding plasma bubble edge after the laser has turned off. The quantitative consistency between experimental data and theoretical prediction provides strong evidence for the occurrence and growth of interchange instabilities. A cutoff relation for stabilization, $m > \sim [8\pi\beta(1 + D_m k_\perp^2 \gamma_{\max}^{-1})]^{1/2}$, has been found in the linear growth regime and was found to match the data. Experimental measurements are important for directly revealing, in a different context, previously unpredicted physical phenomena. They indicate the fundamental importance of 3D processes in certain regimes and provide invaluable information for benchmarking 3D code development.

ACKNOWLEDGMENTS

The work was performed at the LLE National Laser User's Facility (NLUF) and was supported in part by U.S. DOE (Grants No. DE-FG52-07NA28059 and No. DE-FG52-06N826203), LLNL (Grants No. B543881 and No. LDRD-ER 898988), LLE (Grant No. 414090-G), and The Fusion Science Center at University of Rochester (Grant No. 412761-G).

[1] H. P. Furth, J. Killeen, and M. N. Rosenbluth, Phys. Fluids **6**, 459 (1963).
[2] B. Coppi, Phys. Rev. Lett. **12**, 6 (1964).
[3] J. P. Freidberg, *Ideal Magnetohydrodynamics* (Plenum Press, New York, 1987).
[4] D. Biskamp, *Magnetic Reconnection in Plasmas* (Cambridge University Press, Cambridge, 2000).
[5] R. P. Drake, *High-Energy-Density Physics* (Springer, New York, 2006).
[6] C. K. Li *et al.*, Phys. Rev. Lett. **99**, 015001 (2007).
[7] C. K. Li *et al.*, Phys. Rev. Lett. **97**, 135003 (2006).
[8] C. K. Li, F. H. Seguin, J. A. Frenje, J. R. Rygg, R. D. Petrasso, R. P. J. Town, O. L. Landen, J. P. Knauer, and V. A. Smalyuk, Phys. Rev. Lett. **99**, 055001 (2007).
[9] C. K. Li *et al.*, Phys. Rev. Lett. **100**, 225001 (2008).
[10] L. Spitzer, *Physics of Fully Ionized Gases* (Interscience Publishers, New York, 1962).
[11] S. I. Braginskii, *Review of Plasma Physics* (Consultant Bureau, New York, 1965).
[12] M. G. Haines, Phys. Rev. Lett. **78**, 254 (1997).
[13] G. B. Zimmerman and W. L. Kruer, Comments Plasma Phys. Contr. Fusion **2**, 51 (1975).
[14] P. D. Nielsen and G. B. Zimmerman, Lawrence Livermore National Laboratory Report No. UCRL-53123, 1981 (unpublished).
[15] R. D. Petrasso *et al.*, Phys. Rev. Lett. (to be published).
[16] J. M. Soures *et al.*, Phys. Plasmas **3**, 2108 (1996).
[17] S. C. Cowley and M. Artun, Phys. Rep. **283**, 185 (1997).
[18] C. K. Li *et al.*, Phys. Rev. Lett. **102**, 205001 (2009).
[19] T. J. Kessler *et al.*, *Laser Coherence Control: Technology and Applications* (SPIE, Bellingham, WA, 1993).
[20] D. D. Meyerhofer *et al.*, Phys. Plasmas **8**, 2251 (2001).
[21] F. H. Séguin *et al.*, Phys. Plasmas **13**, 082704 (2006).
[22] The effects of scattering on proton deflection are minimum due to the negligible energy loss as those 15 MeV backlighting protons passing through the plasmas ($\rho L \sim 0.5$ mg cm^{-2}) [25,26].
[23] M. M. Marinak *et al.*, Phys. Plasmas **8**, 2275 (2001).
[24] S. E. Widnall, D. B. Bliss, and C. Tsai, J. Fluid Mech. **66**, 35 (1974).
[25] C. K. Li and R. D. Petrasso, Phys. Rev. Lett. **70**, 3059 (1993).
[26] V. L. Highland, Nucl. Instrum. Methods **129**, 497 (1975).